ACS EARTH AND SPACE CHEMISTRY

http://pubs.acs.org/journal/aesccq

Article

Experimental Coupling of a MEMS Gas Chromatograph and a Mass Spectrometer for Organic Analysis in Space Environments

Ryan C. Blase,* Mark J. Libardoni, Gregory P. Miller, Kelly E. Miller, Charity M. Phillips-Lander, J. Hunter Waite, Christopher R. Glein, Hongbo Zhu, Abhishek Ghosh, Anandram Venkatasubramanian, Xudong Fan, and Katsuo Kurabayashi

Cite This: *ACS Earth Space Chem.* 2020, 4, 1718−1729

Read Online

ACCESS | Metrics & More | Article Recommendations | Supporting Information

ABSTRACT: The mass spectrometer for planetary exploration (MASPEX) is a versatile mass spectrometer with unprecedented mass resolution designed for spaceflight. However, the current version of MASPEX is designed for continuous sampling during flybys of planetary bodies and does not include gas chromatography, which can improve the analysis of complex mixtures of organic compounds in space environments. Here, micro-electro-mechanical system (MEMS) gas chromatography (GC) linearity, reproducibility, and column analytical performance were first demonstrated prior to the coupling to MASPEX for MEMS GC−mass spectrometer (MS) analyses. Linearity of response was demonstrated for *n*-hexane over 2 orders of magnitude of on-column mass (concentration). Retention time reproducibility in the MEMS GC was ≤2% relative standard deviation (RSD). MEMS GC column analytical performance calculations showed the average number of theoretical plates, *N*, and the height equivalent to a theoretical plate, HETP, to be 16 239 (1623 plates per meter) and 0.062 cm, respectively. *N* defines a chromatographic centroid peak apex divided by the peak width at half height, similar to mass resolution. When coupled to MASPEX, the retention time reproducibility was in a similar range of 1−2% relative standard deviation with a slightly larger deviation seen from the mass spectrometer detector due to start trigger variations with a manual start trigger in the FastFlight software compared to the LabView code used for the MEMS GC−MS testing. The collected mass spectra showed close consistency with National Institute of Standards and Technology (NIST) reference mass spectra providing confidence in chemical compound identification. We present the first data generated from the coupling of these devices.

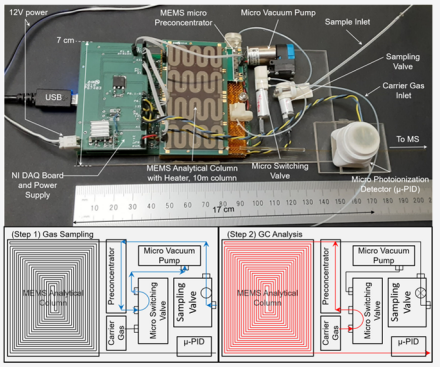

INTRODUCTION

Mass spectrometers (MS) have long been regarded as the "gold standard" in analytical chemistry for chemical compound identification. However, as sample matrix complexity increases a variety of near isobaric and sometimes completely isobaric ion interferences congest the mass spectrum. These interferences make deconvolution of the mass spectrum difficult, at best, and more often than not, impossible. Separation science then comes to the rescue. The separation of complex sample matrix components prior to mass spectrometry analysis provides a powerful analytical tool. Various separation science capabilities in conjunction with continuous improvements in mass accuracy, mass resolution, selectivity, and sensitivity have further solidified this gold standard reputation in a variety of analytical applications (Table 1).

Gas chromatography (GC), the main separation science capability that is the focus of this paper, has been employed for decades. In space science, GC has been used for atmospheric composition measurements in the missions Pioneer Venus[14] and Venera 11 and 12.[15] The use of mass spectrometers (MS) in space missions has been well documented in three review articles.[16−18] In the laboratory, GC was coupled with MS in 1955 and 1956, with publications on these works appearing in 1957[2] and 1959.[3] GC−MS has also been employed in space science investigations including Viking,[19] Cassini−Huygens,[20] Ptolemy on the Philae Lander as part of Rosetta,[21] and Sample Analysis at Mars (SAM), part of the Mars Science Laboratory[22] on Curiosity. One promising, upcoming work is a GC−MS to investigate volatile species in the lunar soil on the Luna−Resurs mission.[23] The GC separation allows for molecular species to be introduced into a mass spectrometer in a nearly compound-by-compound fashion, much like a single file line. The orthogonality of the two separation mechanisms improves the ability to identify specific compounds and determine precisely their abundances by increasing resolution, sensitivity, selectivity, and hence detectability.

Received: May 15, 2020
Revised: July 31, 2020
Accepted: August 26, 2020
Published: August 26, 2020

https://dx.doi.org/10.1021/acsearthspacechem.0c00131
ACS Earth Space Chem. 2020, 4, 1718−1729

Table 1. Separation Science Methods, Their Inception or Invention Year, the Year of Inception with Mass Spectrometry, and Their Impact on Analytical Applications Today

separation science method	inception	inception with mass spectrometry	gold standard application
gas chromatography	1952[1]	1955–1956[a] 1957;[2] 1959[3]	forensics, sports antidoping, oil and natural gas, food, flavors, beverage, perfume analysis
liquid chromatography	1941[4]	1969[5] 1972;[6] 1973[7,8]	metabolomics, clinical and forensic toxicology, drug screening
capillary electrophoresis	1937[9]	1987[10]	proteomics (post-translationally modified peptides and proteins)
ion mobility spectrometry	1896,[11] 1900[12]	1962[13]	proteomics (gas-phase protein structure), trace explosives detection (homeland security applications)

[a]Two separate efforts were performed: McLafferty and Gohlke with a gas chromatograph (GC) and Bendix mass spectrometer developed by Wiley and Holmes; Morrell with a mass spectrometer from Consolidated Engineering Corp. in 1955–1956. The published papers, 1957 and 1959, after these initial efforts are displayed in the table.

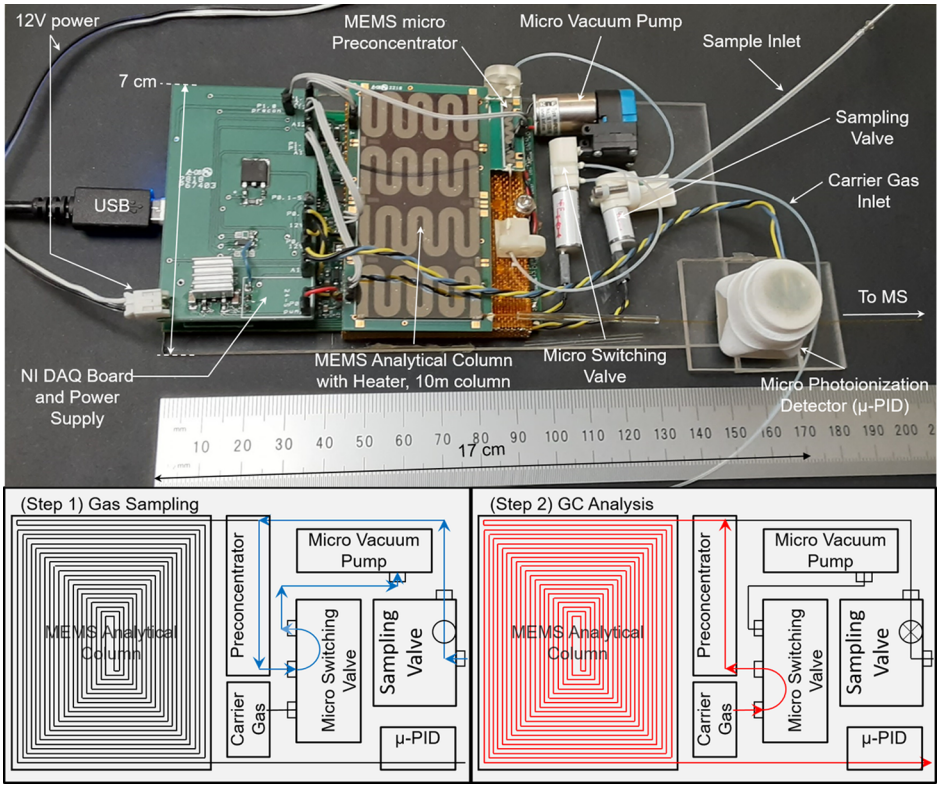

Figure 1. Photograph of the MEMS GC device (top) with the major components labeled. Block diagrams show (step 1) gas sampling with pathway in blue (bottom left) and (step 2) GC analysis with carrier gas pathway in red (bottom right) to illustrate operation. The black lines show portions of pathways not being used.

The micro-electro-mechanical system (MEMS) GC technology described in this work has been developed at the University of Michigan. Microfabricated GC columns at the University of Michigan began in the laboratory of Richard Sacks.[24] Further developments of microfabricated GC columns have continued in the laboratories of Katsuo Kurabayashi and Xudong Fan.[25−27] These systems have extended to different detectors,[28−31] multidimensional micro GC−GC systems (two-dimensional (2D)[32] and three-dimensional (3D)[33] systems), microinjectors (preconcentrators),[34,35] and micro thermal modulators.[36] We have previously demonstrated the analytical utility of multidimensional gas chromatography for in situ investigations of multiple harsh environments.[37,38] In this paper, work focuses on an adaptation for GC−MS of a MEMS micro GC equipped with a 10 m long rectangular (150 μm × 240 μm) analytical column and micro-photoionization detector (μ-PID) at the GC analytical column exit.

The mass spectrometer for planetary exploration (MASPEX) is a multibounce time-of-flight (MBTOF) mass spectrometer with unprecedented high mass resolution capability for spaceflight.[39] MASPEX incorporates variable ion flight length, which allows to adjust the mass resolution as needed. Because of its mass resolution and sensitivity, MASPEX will be on the payload of NASA's Europa Clipper, a flyby mission investigating the composition and habitability of Europa, a moon of Jupiter. Our team is continuing to develop this technology for future landed missions, including a potential Europa Lander mission under the Instrument Concepts for Europa Exploration-2 (ICEE-2) program.[40]

There are numerous other, scientifically rich destinations in the solar system.[41] By enhancing capabilities to identify specific components of complex natural mixtures, future MASPEX implementations that include the MEMS GC have the potential to provide further insight into the habitability[42] and potential presence of isotopic and organic biomarkers[43] at

https://dx.doi.org/10.1021/acsearthspacechem.0c00131
ACS Earth Space Chem. 2020, 4, 1718−1729

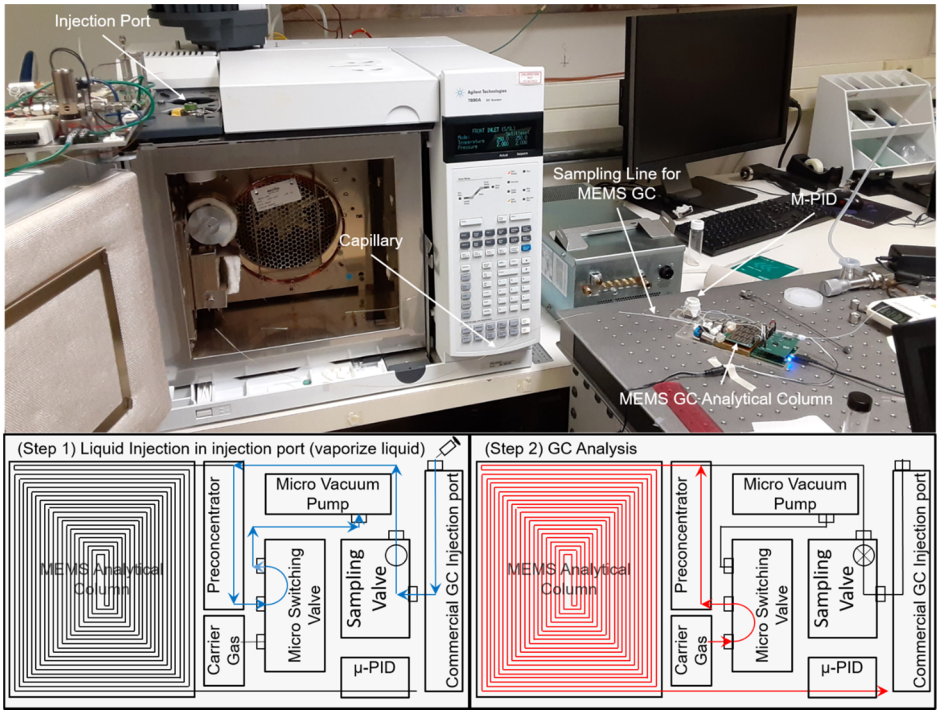

Figure 2. Photograph of the experimental setup for the linearity of response experiments with *n*-hexane. The block diagrams show (step 1) liquid injection into the injection port to vaporize the sample and push the sample gas through the gas sampling pathway in blue and (step 2) GC analysis with carrier gas pathway in red.

Enceladus, a moon of Saturn, as well as advance understanding of the complex organic chemistry on Mars.[44] Titan, another moon of Saturn, has lakes and seas of liquid hydrocarbons,[45] which may have accumulated significant amounts of other organics that formed in its atmosphere. Moreover, the application of the MEMS GC with MASPEX at small body targets will be able to improve our understanding of solar system formation and its evolution. As an example, the ROSINA mass spectrometer aboard the Rosetta spacecraft indicated a diversity of organic compounds in comet 67P/Churyumov–Gerasimenko.[46,47] The ALICE instrument aboard New Horizons found that Pluto has a chemically complex atmosphere that includes methane, ethane, acetylene, and ethylene.[48,49] Additional studies of comets, asteroids, and Pluto and other Kuiper Belt objects over the coming decades will provide key insight into the organic complexity of icy worlds.

■ EXPERIMENTAL SECTION

The MEMS GC analytical column has a rectangular channel with dimensions 150 μm × 240 μm and an overall length of 10 m. The MEMS GC device is displayed in Figure 1 with major components labeled. Gas sampling (step 1 in Figure 1 bottom left), normally of volatile organic compounds, is accomplished via the sample inlet. The sampling valve opens and the microswitching valve switches to allow the micro vacuum pump to draw the sampled gases across the preconcentrator, which is filled with sorbent materials Carbopack B and X, for a fixed amount of time. The gas sampling pathway is depicted by the blue lines and arrows. Once the sampling time has been reached, the sampling valve closes and the microswitching valve switches back to allow the helium carrier gas to push through the preconcentrator and the analytical column. This is depicted as step 2, GC analysis, with the carrier gas pathway in red in the bottom right portion of Figure 1. A user-defined waiting time is employed to allow equilibration of the helium carrier gas through the analytical column. After the waiting time has been reached, two voltage pulses are applied via pulse width modulation to the preconcentrator to desorb the trapped volatile species. The first pulse serves to rapidly heat the preconcentrator and the second pulse serves to hold the preconcentrator at the desired desorption temperature to provide a narrow sample plug of analyte to the analytical separation column. Once injected, the vaporized species separate in the analytical column via interactions with the stationary phase. As the separated components elute from the analytical column, they pass by a micro-photoionization detector (μ-PID), where a signal response can be registered. For the MEMS GC–MS experiments, a guard column transfer line with an inner diameter of 250 μm is connected after the μ-PID and leads directly into the ion source of the MBTOF mass spectrometer.

Linearity of Response. For experiments to measure the linearity of response, the MEMS GC sample inlet was connected to an Agilent 7890 commercial GC injector inlet through a capillary column. A photograph of this experimental setup is displayed in Figure 2. Liquid samples were manually injected into the commercial injection port (step 1 in Figure 2) at an inlet temperature of 250 °C and a helium inlet pressure of ~115 000 Pa (16.7 psia or 2 psig) to sweep the vaporized sample to the MEMS GC sample inlet and across the preconcentrator. Gas sampling was performed for 30 s to ensure that the entire sample plug from the injector was swept by helium and trapped on the preconcentrator. The sampling valve was closed and the microswitching valve was switched to provide helium carrier gas flow to the analytical column for GC analysis (step 2 in Figure 2). A 6 s waiting (or equilibration) time after switching the valve was used prior to desorbing the

https://dx.doi.org/10.1021/acsearthspacechem.0c00131
ACS Earth Space Chem. 2020, 4, 1718–1729

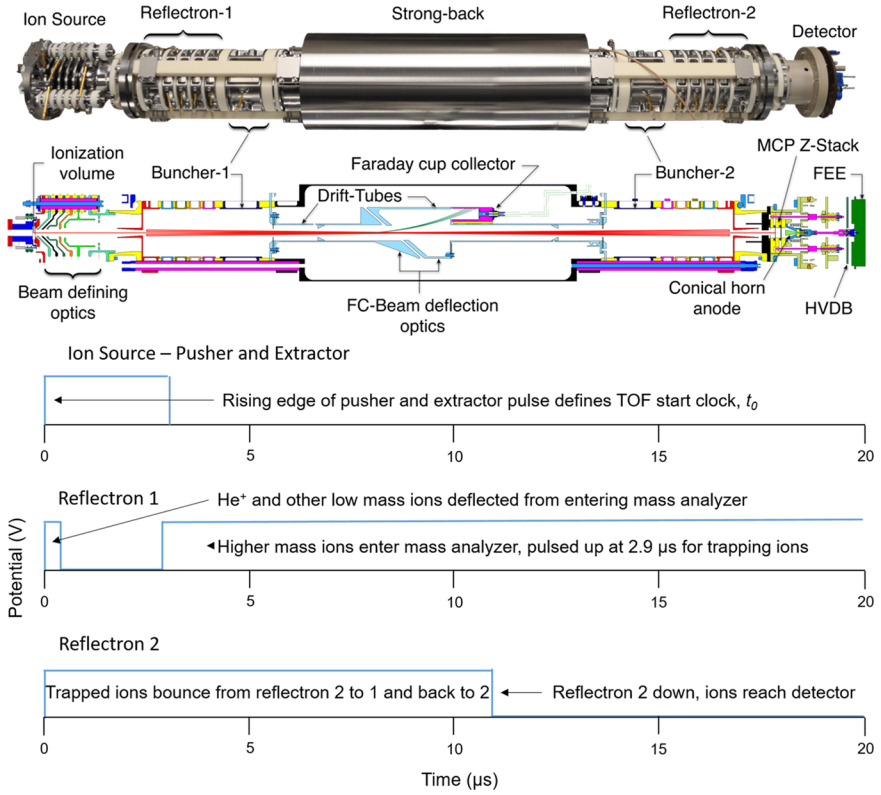

Figure 3. MASPEX instrument that utilizes multibounce time-of-flight (MBTOF) to lengthen the ion separation distance to achieve high-resolution measurements. The time sequence diagram for instrument operation with the MEMS GC is displayed in the bottom portion.

sample off the preconcentrator. The preconcentrator was then rapidly heated with a high-voltage pulse for a duration of 0.8 s to approximately 250−300 °C and then held at that temperature with a second, lower-voltage pulse for 8 s. The initial high-voltage pulse of the preconcentrator defines the injection start time of the analytes onto the analytical column. The column temperature profile was isothermal at 17.5 °C for the first 75 s after injection and then heated at a rate of approximately 14.7 °C min^{-1} from 75 to 130 s and 10.3 °C min^{-1} from 130 to 300 s. The detector for these experiments was the μ-PID as displayed in Figures 1 and 2. Dilutions of *n*-hexane were performed with dichloromethane (DCM) as the solvent to generate a calibration curve. Six sample concentrations with quadruplicate manual injections at each concentration were performed with concentrations ranging from 6.55×10^{-3} down to 2.05×10^{-4} g mL^{-1}. This results in an on-column mass of 4.91×10^{-6} down to 1.54×10^{-7} g per 1 μL injection. The calibration curve showed the peak area response (in V·s) of the μ-PID versus the on-column injection mass, or concentration in grams.

Individual Alkane and Alkane Mixture Injections on the MEMS GC. A series of alkanes were run individually on the MEMS GC and then run as a mixture to test the retention time reproducibility. The alkanes run were *n*-pentane, hexanes (3-methylpentane, *n*-hexane, cyclohexane), *n*-heptane, *n*-octane, *n*-nonane, and *n*-decane. Hereafter, we will refer to these as C_5−C_{10}. For these tests, the helium carrier gas flow rate was 1.2 mL min^{-1}. The headspace vapor was drawn through the sample inlet using the micro vacuum pump for varying amounts of time up to 6 s. The microswitching valve then switched to allow helium to flow again through the preconcentrator and the analytical column. A 6 s delay time, or equilibration time, was used to allow helium to flow through the preconcentrator and analytical column prior to the heating of the preconcentrator. The preconcentrator was then rapidly heated with a high-voltage pulse for a duration of 0.8 s to approximately 250−300 °C and then held at that temperature with a second, lower-voltage pulse for 8 s. The initial high-voltage pulse of the preconcentrator defines the injection start time of the analytes onto the analytical column. The column temperature profile was isothermal at 17.5 °C for the first 75 s after injection and then heated at a rate of approximately 14.7 °C min^{-1} from 75 to 130 s and 10.3 °C min^{-1} from 130 to 300 s. The detector for these experiments was the μ-PID.

Alkane Mixture Injections for the MEMS GC−MS Experiments. The MEMS GC was later connected to a prototype of the MASPEX instrument, MBTOF 3, through a guard column and heated transfer line that was attached after the μ-PID detector. In these MEMS GC−MS experiments, the flow rate was decreased to reduce the helium carrier gas load into the vacuum of the mass spectrometer. However, the helium carrier gas velocity still increased overall due to the vacuum outlet into the mass spectrometer, shifting the retention times to shorter retention times relative to experiments exhausted into the air. Headspace vapor sampling time and helium equilibration time remained the same (6 s) as in the first set of experiments with only the MEMS GC. Preconcentrator settings and GC column temperature settings also remained the same.

One major difference for the MEMS GC−MS experimental setup, relative to just the MEMS GC, was the use of two different software platforms controlling the two devices. The MEMS GC and μ-PID detector are controlled by LabView and are triggered by a user hitting the run button. MASPEX is

https://dx.doi.org/10.1021/acsearthspacechem.0c00131
ACS Earth Space Chem. 2020, 4, 1718−1729

controlled by a FastFlight 12 bit analog-to-digital converter (ADC) operating at a sampling frequency of 2 GHz (0.5 ns time-of-flight (TOF) bin width), also requiring a user to hit the start button for the data acquisition software to begin. The two sets of software were triggered individually, resulting in a slight time delay between the start trigger of the two programs. The time delay was synchronized to the best consistency possible for a manual start. Chromatographic data were taken with the μ-PID from the LabView software and the microchannel plate (MCP) detector from the FastFlight software. The FastFlight software contains a total ion chromatogram (TIC) window that averages the ion counts across all of the bins of the mass spectrum over a defined number of mass spectra, in this case 500 spectra, and records those counts in the TIC. Mass spectral data, 500 averaged mass spectra per data point, can be accessed by clicking across the data points of the TIC. Chromatographic data are presented for the MEMS GC−MS experiments as recorded by the μ-PID and the MASPEX MCP detector from the total ion chromatogram window from the FastFlight software.

Operation of MASPEX Mass Spectrometer for MEMS GC−MS Experiments. The MASPEX MBTOF and its operation have been described in detail previously,[39] so only a brief summary is provided here. MBTOF enables ions to travel long distances, providing increased mass resolution, in a compact instrument by folding the flight path. It consists of two opposing electrostatic reflectrons (R1, R2) that bounce the ions in an electrostatic trap, associated buncher lenses, drift tube, and ion optics that couple the ion source to the detector (Figure 3). Ions are generated by electron ionization (EI) in the ionization volume, a field-free region, defined by two parallel high-transmission-gridded electrodes, the pusher and extractor, held at ground potential. Electron paths follow tight helical trajectories resulting from two collimating magnets. The helical electron path increases the neutral−electron interaction time to improve ionization efficiency and generates a weak space-charge potential well that stores ions (storage ion source), improving source sensitivity.[50] To extract the ions into the TOF analyzer, we apply two independent, fast, push/pull pulses (~5 ns rise-time for 3 μs) to energize the pusher grid with a more positive voltage relative to the extractor grid and provide constant energy per charge acceleration. The ion packet is accelerated out of the ion source and a series of beam defining optics guides the ions into the mass analyzer. When first injected into the mass analyzer, R1 is off and R2 is on (potential exceeds the ion extraction potential). After the extracted ions have passed by R1 it is energized, or turned on. The ions enter into the drift tube and are reflected by R2 (bounced back toward R1). The ions are trapped between R1 and R2, dispersing in time according to mass ($t \sim m^{1/2}$), increasing flight length and flight time with each bounce. Because the reflectrons are gridless and the ion mean free path is much longer than even many reflected lengths of the MBTOF flight path, there is minimal ion packet spreading and loss. To maintain stable ion trajectories inside the analyzer, two ion bunchers have been fitted on each of the reflectron elements that provide transverse focusing of the ion packets during multiple bounces. After a user-determined time has been reached, R2 turns off and the ions are released to the microchannel plate (MCP) detector. The extraction, trapping, and mass analysis are performed at kHz rates to enable detection of fast elution of gas chromatography peaks.[51]

For the MEMS GC−MS experiments, the MBTOF mass spectrometer (Figure 3) is operated in a two bounce (three passes or lengths of the analyzer) mode. This mode provides increased mass resolution but reduces the collected mass range versus linear mode, where the entire mass range is collected per extraction. Ions are generated in the storage ion source under the following conditions: electron energy of 35 eV, electron emission current of 100 μA (collector current of 30−40 μA due to elevated 10^{-3} Pa (10^{-5} Torr) pressure from helium carrier gas), and extraction rate of 10 kHz using the FastFlight data acquisition software as the trigger. The reduced electron energy of 35 eV was used to decrease the ionization of helium in the ion source. The pusher and extractor of the ion source were pulsed for a duration of 3 μs. The rising edge of this pulse defines the ion injection and hence start clock for the time-of-flight. Ions exit the source, but for the first 400 ns (0.4 μs), the potential on R1 deflects ions from entering the drift tube. The main reason for deflecting (blanking) low mass ions is to eliminate the large helium carrier gas ion signal from the mass spectrum and reduce unnecessary charge extraction from the MCP detector. After this time interval, R1 is pulsed down to allow ions into the drift tube; these ions are then reflected by R2 to increase the flight length and hence the mass resolution. R1 is left down for 2.5 μs and then pulsed up to reflect the ions back toward R2 and the detector. Before these ions arrive at the detector, R2 is pulsed down 11 μs after ion injection and all of the ions are allowed to strike the detector. Due to the timing of the reflectrons, ion masses that arrive at the detector are found in the mass range between 40 and 140 Da. A time sequence diagram is displayed at the bottom portion of Figure 3 to clarify the operation of the mass spectrometer.

RESULTS

Linearity of Response. This experiment was performed to test for linear performance in terms of analyte sampling and desorption with the preconcentrator as a function of analyte concentration, or on-column mass. This experiment is not an investigation of the sensitivity of the μ-PID as these studies have been published previously.[30] The volume of n-hexane per 1 μL manual injection considering dilution in dichloromethane (DCM) and the density of *n*-hexane were used to calculate the on-column mass. Peak areas in units of V·s were integrated over the peak width at the base. Results of the linearity of response experiments for *n*-hexane are displayed in the log−log plot of Figure 4. The best fit is a power law ($y = a*x^b$) with the exponent, b, near unity, which represents a linear relationship. Thus, the data show relatively close consistency with a linear relationship over 2 orders of magnitude dynamic range, with a correlation coefficient (R^2) value of 0.9980. Variations in injection volume due to manual injections are the most likely cause for the error in the measurement, especially for the highest concentration data point. The removal of this data point improves the linear fit, yielding a correlation coefficient (R^2) value of 0.9999. A linear fit to the same data on a nonlogarithmic scale is displayed in Figure S1 of the Supporting Information.

Individual Alkane Injections on the MEMS GC. Multiple samplings and injections were performed to determine the retention times for each of the individual alkanes, and the results are presented in Table 2. The individual alkane injections are also plotted together in Figure 5. As mentioned in the Experimental Section, sampling times

https://dx.doi.org/10.1021/acsearthspacechem.0c00131
ACS Earth Space Chem. 2020, 4, 1718−1729

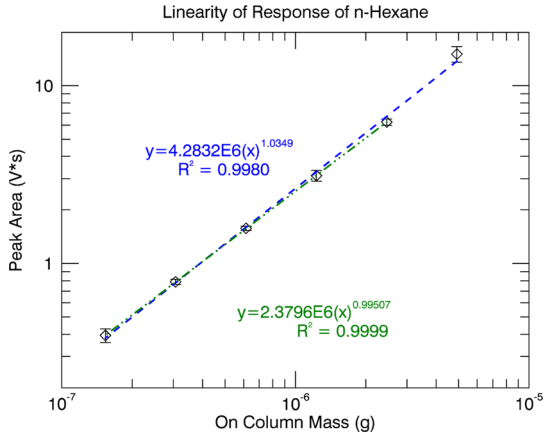

Figure 4. Linearity of response data in peak area (V·s) versus on-column mass (g) shown as black diamonds for *n*-hexane measured by the μ-PID with the experimental setup displayed in Figure 2. The best fit line, with equation, is shown in blue. The best fit line, with equation, removing the highest concentration data point is shown in green.

Table 2. Retention Time Reproducibility for the Individual Alkane Injections on the MEMS GC

analyte	number of injections	average R.T. (s)	standard dev. RT (s)	% RSD
n-pentane	7	39.91	0.24	0.60
3-methylpentane	6	50.68	0.34	0.67
n-hexane	6	54.43	0.56	1.03
cyclohexane	6	61.60	0.46	0.75
n-heptane	10	90.26	1.62	1.79
n-octane	6	138.25	0.82	0.59
n-nonane	6	186.74	1.57	0.84
n-decane	6	246.27	4.5	1.83

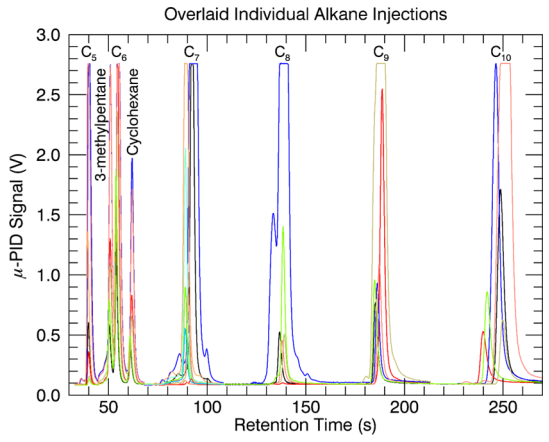

Figure 5. Overlaid individual alkane injections corresponding to results in Table 2.

of the analyte were varied up to 6 s to vary the concentration of the analyte and investigate any effects of sample concentration on the retention time reproducibility. The heating rates of 14.7 °C min^{-1} from 75 to 130 s and 10.3 °C min^{-1} from 130 to 300 s were not perfectly linear and the column temperature profiles for the individual and mixture injections are displayed in Figure S2 of the Supporting Information. The average heating rate from 75 to 300 s was 11.4 °C min^{-1}. Retention time reproducibility showed percent relative standard deviation (% RSD) values of ≤2% for all of the individual alkane injections.

Peak broadening can be seen at higher concentrations in Figure 5 and subsequent figures. Peak broadening results mainly from one, or the combination, of two effects: (1) injection peak width at the preconcentrator; (2) sample overloading of the stationary phase. The first effect is due to the physical size, or length, of the preconcentrator. As sample concentration increases, more sites along the length of the preconcentrator are filled thereby increasing the length, and hence sample width, of the sample plug upon thermal desorption. The second effect is due to sample overloading of the stationary phase that results in fronting, or shoulders, preceding the main peak and significant tailing of the peak. This is evident for the chromatographic signals in Figure 5 where the peak is flat-topped, indicating that the μ-PID detector is saturated (the dynamic range has been exceeded). These two effects are common in gas chromatography, and the MEMS GC shows that retention time reproducibility is still quite good even with high sample concentrations.

Alkane Mixture Injections on the MEMS GC. A mixture of the six straight-chain alkanes, C_5−C_{10}, including the isomers of hexane (C_6), was then prepared to test the retention time reproducibility of the MEMS GC and make a comparison to the individual analyte runs. The mixture was sampled in the same way, and the helium carrier gas flow rate and column oven temperature profile were also consistent with the individual alkane runs. Five injections of the alkane mixture with sampling times up to 6 s, to vary concentration, were performed to investigate retention time reproducibility and the results are presented in Table 3. The overlaid chromatograms

Table 3. Retention Time Reproducibility for the Alkane Mixture Injections on the MEMS GC

analyte	number of injections	average R.T. (s)	standard dev. RT (s)	% RSD
n-pentane	5	39.23	0.27	0.70
3-methylpentane	5	50.23	0.27	0.55
n-hexane	5	53.93	0.38	0.70
cyclohexane	5	61.18	0.38	0.62
n-heptane	5	91.12	0.51	0.56
n-octane	5	141.48	1.04	0.73
n-nonane	5	191.78	1.95	1.01
n-decane	5	248.33	3.52	1.42

are also displayed in Figure 6. Retention time reproducibility for the alkane mixture injections showed % RSD values at ≤1.5%. The RSD value of the MEMS GC (∼1%) is an order of magnitude larger than that of the Agilent GC system (0.1%). The commercial GC system incorporates electronic pneumatics control with real-time ambient pressure and temperature compensation. This typically results in the high retention time reproducibility of the commercial GC. The absence of such sophisticated pneumatics control may cause the MEMS GC to yield the higher RSD value.

To determine the MEMS GC column analytical performance, calculations were performed to determine the number of theoretical plates, *N*, and the height equivalent to a theoretical plate, HETP, based on the eluting chromatographic peak widths. The idea of theoretical plates stems from distillation chromatography (fractional distillation), where the plates or trays represented a region where equilibrium was reached

https://dx.doi.org/10.1021/acsearthspacechem.0c00131
ACS Earth Space Chem. 2020, 4, 1718−1729

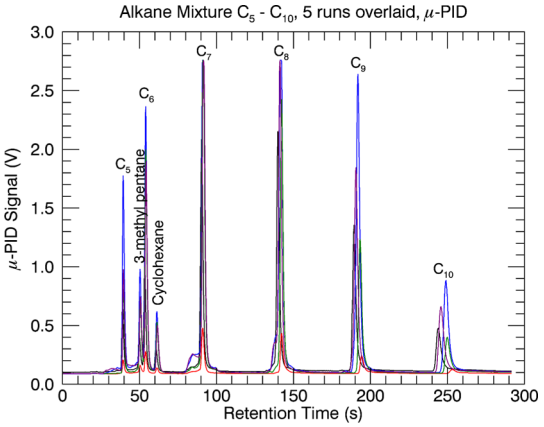

Figure 6. Five overlaid injections of the C_5−C_{10} alkane mixture corresponding to Table 3.

between the vapor and liquid phases. For GC and other forms of chromatography a hypothetical stage, or zone, where vapor and liquid phases of the analyte reach equilibrium are considered a theoretical plate. The efficiency of the separation increases with the number of theoretical plates. The height equivalent to a theoretical plate, HETP, provides a numerical representation of the length of the column divided by the number of theoretical plates (L/N). The equation used for the calculation of N was as follows

$$N = 5.545 \times \left(\frac{t_R}{W_{0.5}}\right)^2$$

where t_R represents the retention time centroid and $W_{0.5}$ stands for the width of the chromatographic peak at half height (or full width at half-maximum). The calculated number of theoretical plates for each eluting analyte from the alkane mixture is displayed in Table 4. For an isothermal separation, the value of N should be similar for all eluting species as evidenced by the first four eluting analytes. Chromatographically speaking, the later eluting species would experience significant band broadening and the much wider peaks would give a similar theoretical plate value but at the expense of separation efficiency. A column temperature program was used to increase the efficiency of the overall separation of the mixture, and as the column temperature increased, the number of theoretical plates, N, showed an increasing trend. For a graphical representation of the analyte retention (elution) time versus the column temperature, see Figure S2 of the Supporting Information. Since the separation was performed with a column temperature ramp, the average number of N and HETP are reported. The average number of theoretical plates, N, was 16 239 and the average height equivalent to a theoretical plate, HETP, was 0.062 cm over the column temperature range of the separation (more information on HETP given in the Supporting Information and Figure S3). Compared to commercial open tubular columns presented from Restek,[52] Agilent,[53] and Supelco[54] of similar column area, the number of theoretical plates per meter is approximately 3890 versus our average at 1623 and maximum of 3704. Moreover, similar values of HETP have been reported as compared to our minimum value of 0.0271 in the literature for square and rectangular GC columns.[55]

Alkane Mixture Injections for the MEMS GC−MS Experiments. The same alkane C_5−C_{10} mixture was then run on the MEMS GC−MS experimental setup to investigate reproducibility and establish the first proof-of-concept performance. The retention times recorded by the μ-PID and the MASPEX microchannel plate (MCP) detector for the MEMS GC−MS experiments are shown in Table 5. The overlaid chromatograms produced from the μ-PID and MCP detector are displayed in Figure 7 and in the Supporting Information, Figure S4, respectively. Six chromatograms were saved from six replicate injections as recorded by the μ-PID detector and five chromatograms from the FastFlight data. One run was unsuccessfully correlated in time, not started with similar time delta between LabView and FastFlight. As mentioned in the Experimental Section, there was a time delay between the start clock of the LabView software and FastFlight software. This time delay was on average 5.4 s (standard deviation of 0.19 s). Retention time reproducibility for the alkane mixture injections in the MEMS GC−MS experiments showed % RSD values being ≤2%. The slightly higher % RSD values recorded by the MCP detector are most likely due to time variations in the manual start trigger of the FastFlight software compared to the LabView software.

Mass spectra were collected at each analyte signal apex from the total ion chromatogram (TIC) providing the largest ion signals for all ions but some signals reaching saturation levels. The mass spectra of 3-methylpentane, *n*-hexane, and cyclohexane from MASPEX are displayed in Figure 8 with the TIC in the top left. These three isomers of C_6 are well separated by the MEMS GC. Identification of these analytes can be confirmed by their mass spectral fingerprint: parent and

Table 4. Calculated Number of Theoretical Plates, *N*, and Height Equivalent to a Theoretical Plate (HETP) to Indicate Column Performance for the Analytes from the Alkane Mixture[a]

analyte	*N*	HETP (cm)	column temp. at time of elution (°C)
n-pentane	5046 ± 75	0.198 ± 0.0030	17.47 ± 0.031
3-methylpentane	6266 ± 424	0.160 ± 0.011	17.50 ± 0.033
n-hexane	7468 ± 270	0.134 ± 0.0049	17.51 ± 0.035
cyclohexane	7317 ± 563	0.137 ± 0.012	17.52 ± 0.032
n-heptane	13 092 ± 2082	0.0779 ± 0.012	22.32 ± 0.17
n-octane	26 066 ± 4534	0.0395 ± 0.0084	35.23 ± 0.41
n-nonane	37 048 ± 2691	0.0271 ± 0.0020	49.06 ± 0.77
n-decane	27 607 ± 2625	0.0365 ± 0.0035	56.82 ± 0.77
average over temp. range	16 239 ± 1658	0.062 ± 0.0063	37.26 ± 0.49

[a]The calculated *N* and HETP are the average of all five mixture runs. The average number of *N* and HETP over the column temperature profile used for the separation are displayed in the bottom row of the table.

https://dx.doi.org/10.1021/acsearthspacechem.0c00131
ACS Earth Space Chem. 2020, 4, 1718−1729

Table 5. Retention Time Reproducibility for the Alkane Mixture Injections on the MEMS GC Coupled with MASPEX, the Mass Spectrometer[a]

analyte	number of injections	average R.T. (s)	standard dev. RT (s)	% RSD
n-pentane	6/5	31.48/26.08	0.11/0.43	0.33/1.64
3-methylpentane	6/5	40.07/34.52	0.19/0.40	0.48/1.15
n-hexane	6/5	42.78/37.37	0.23/0.54	0.53/1.43
cyclohexane	6/5	48.53/43.03	0.28/0.41	0.57/0.96
n-heptane	6/5	74.13/68.65	0.94/1.20	1.27/1.75
n-octane	6/5	122.81/117.34	0.94/1.26	0.77/1.07
n-nonane	6/5	171.00/165.57	1.35/1.41	0.79/0.85
n-decane	6/5	220.32/215.38	2.05/2.13	0.93/0.99

[a]These MEMS−GC−MS runs capture the retention times recorded by the μ-PID (values left of forward slash) and the MASPEX MCP detector (total ion chromatogram from the FastFlight data acquisition software).

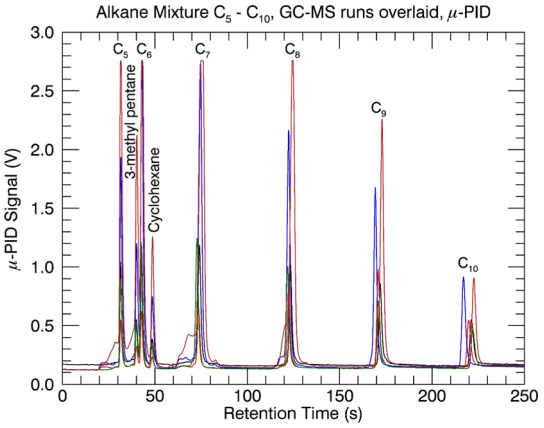

Figure 7. Overlay of six alkane mixture injections detected by the μ-PID in the MEMS GC−MS analysis.

fragment ion abundances that provide diagnostic information on the chemical structure (Table 6). For instance, 3-methylpentane and *n*-hexane share the same chemical formula of C_6H_{14} (average molecular weight = 86.175 Da, monoisotopic mass = 86.10955 Da), while cyclohexane has a chemical formula of C_6H_{12} (average molecular weight = 84.1597 Da, monoisotopic mass = 84.0939 Da). This mass difference of the parent ion is the simplest diagnostic, and cyclohexane is readily identified as the last compound to elute of the C_6 isomers (labeled with the red asterisk in Figure 8). While not needed for identification, the ion fragmentation patterns including relative abundance trends for m/z 41, 42, 43, 56, and 69 (Table 6) improve confidence in the assignment. Both the National Institute of Standards and Technology (NIST)[56,57] database and MASPEX relative abundances of m/z 41−43 show a stairstep decrease, m/z 56 is 100% in NIST and nearly that in MASPEX, and m/z 69 is

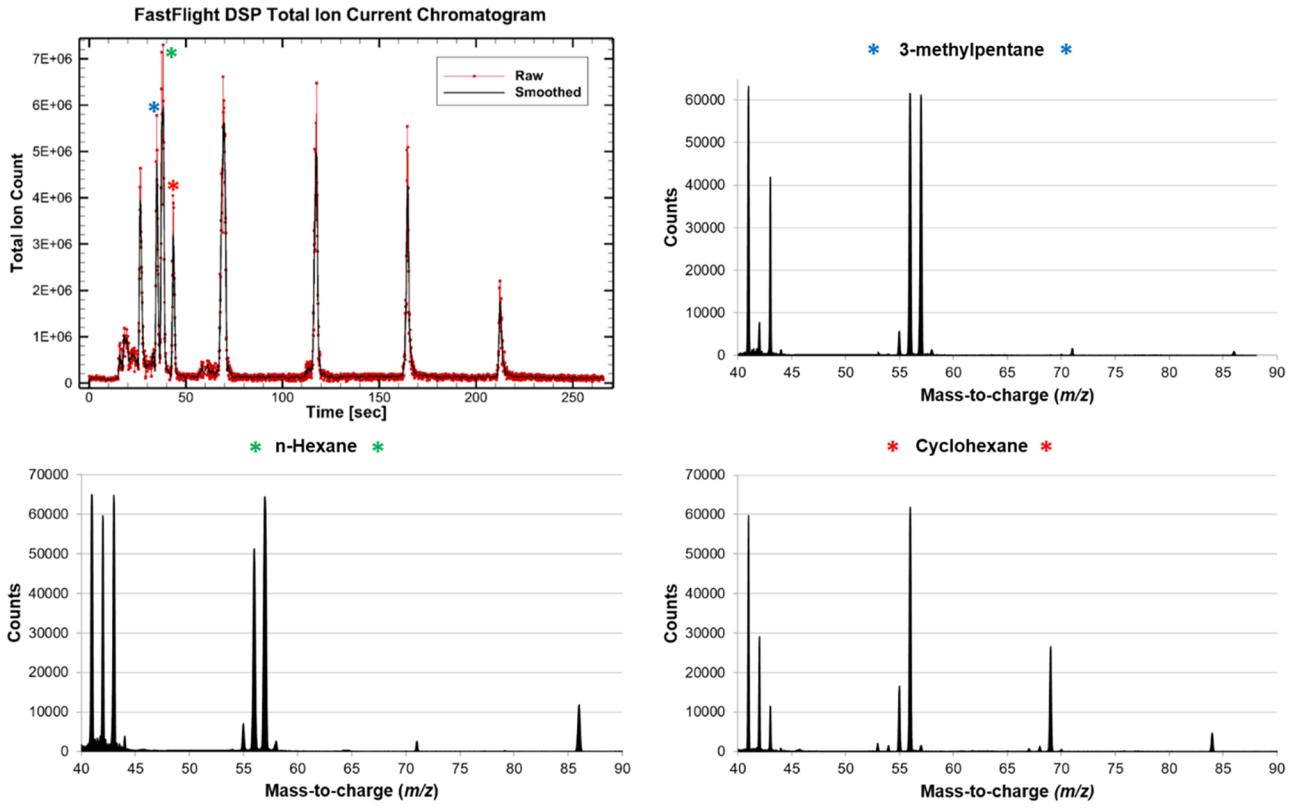

Figure 8. Mass spectra of the three isomers of C_6: 3-methylpentane, *n*-hexane, and cyclohexane detected by MASPEX.

https://dx.doi.org/10.1021/acsearthspacechem.0c00131
ACS Earth Space Chem. 2020, 4, 1718−1729

Table 6. Selected Ion (Parent and Fragment) Relative Abundance Values (Peak Heights) of the C_6 Isomers from their NIST Reference Mass Spectrum Standards at 70 eV Ionization Energy Versus the Abundance Values Acquired from MASPEX at 35 eV Ionization Energy Prior to Saturation

normalized relative abundance of NIST reference versus MASPEX (this work) data						
	3-methylpentane		*n*-hexane		cyclohexane	
ion	NIST	MASPEX	NIST	MASPEX	NIST	MASPEX
86	3%[b]	1%[b]	15%[b]	3%[b]	N/A	N/A
84	N/A	N/A	N/A	N/A	82%[b]	6%[b]
69	N/A	N/A	N/A	N/A	31%	38%
57	100%[a]	60%	100%[a]	51%	5%	2%
56	77%	62%	45%	33%	100%[a]	97%
43	25%	40%	81%	81%	9%	16%
42	4%	10%	41%	44%	20%	40%
41	53%	100%[a]	70%	100%[a]	50%	100%[a]

[a]100% relative abundance is base peak (most abundant ion species in the mass spectrum). [b]Parent (or molecular) ion species. All other ions in the table are fragment ions.

31% in NIST and 38% in MASPEX. Signals at m/z 84 and 69 are not found in the mass spectra of either 3-methylpentane or *n*-hexane, and their trends at m/z 41−43 and 56 and 57 are significantly different.

To discriminate between 3-methylpentane and *n*-hexane, parent and fragment ion abundances must be investigated. According to the NIST reference mass spectra, the parent ion abundance differs between these two species with 3% relative abundance in 3-methylpentane versus 15% relative abundance in *n*-hexane. MASPEX data showed relative abundance values of 1% for 3-methylpentane and 3% for *n*-hexane. Further confidence in identification can be found in fragment ion abundances from m/z 41−43 and 56 and 57 (Table 6). The large discrepancy in abundance between fragment ions at m/z 41 and 42 for 3-methylpentane and the more similar abundances between 56 and 57 are seen in the top right mass spectrum identifying 3-methylpentane as the first isomer to elute from the GC column (labeled with blue asterisk in Figure 8). The more similar abundances expected for fragment ions at m/z 41−43 and difference in abundance between 56 and 57 are seen in the lower left mass spectrum identifying *n*-hexane as the second isomer to elute (labeled with green asterisk in Figure 8).

It should be noted that ion abundance differences between MASPEX mass spectra and NIST reference spectra are expected due to the following: (1) difference in electron energy with our experiment at 35 eV and NIST reference spectra at 70 eV; (2) ion source and overall mass spectrometer instrument geometry differences. Rigorous tuning of the MASPEX instrument could be performed in an attempt to more closely match the NIST reference standards similar to reference compound standards developed by the EPA for calibrating ion abundance measurements in GC−MS systems.[58] However, the spectra reported provide confident analyte identification, and reference compound calibration is not the main focus of this paper.

The mass spectra for the other analytes from the alkane mixture (*n*-pentane, *n*-heptane, *n*-octane, *n*-nonane, and *n*-decane) are presented in the Supporting Information, Figure S5. The mass spectral trends (parent and fragment ion abundances) for the other alkanes are similar to the NIST reference mass spectra as previously discussed in depth for the isomers of C_6. For comparative purposes, mass spectra of all eight compounds in the alkane mixture are plotted versus the NIST reference mass spectra in the Supporting Information, Figure S6. The NIST relative abundance data were normalized to the base peak seen in each mass spectrum from the MASPEX data to provide similar ion count scale windows. Mass resolution values calculated from the mass spectra ($R = m/\Delta m_{fwhm}$) are on average 380, with resolution increasing as the ion mass increases. These resolution values are respectable considering the elevated pressure in the analyzer due to the helium carrier gas. Improvements could be made in the future utilizing a gas jet separator to reduce the helium carrier gas load into the mass spectrometer. Mass resolution could be increased by increasing the flight length (number of bounces) but at the expense of truncating the collected mass range.

CONCLUSIONS

The first successful coupling and proof-of-concept performance validation of the MEMS GC and MASPEX was achieved. MEMS GC linearity, reproducibility, and column analytical performance were first demonstrated prior to the coupling to MASPEX for MEMS GC−MS analyses. MEMS GC linearity was observed over 2 orders of magnitude dynamic range (on-column mass) with a high R^2 value of 0.9980. MEMS GC retention time reproducibility was seen to be at or below 2% RSD for individual alkane injections and alkane mixture injections. The column analytical performance in terms of number of theoretical plates, *N*, and the height equivalent to a theoretical plate, HETP, was found to be 16 239 (1623 plates per meter) and 0.062 cm on average over the column temperature range of the separation. MEMS GC−MS analyses showed very little change in retention time reproducibility (% RSD) values verifying successful proof-of-concept performance of the hyphenated separation technique. Mass spectra produced from MASPEX in the MEMS GC−MS analyses confidently identified each analyte with the structural chemical fingerprint closely resembling what is expected when comparing to the NIST reference mass spectra.

The MEMS GC provides reduced size, weight, and power (SWaP) compared to traditional GC analytical columns previously used in spaceflight applications, and MASPEX provides high mass resolution and high mass accuracy measurements compared to previous spaceflight heritage mass spectrometers. The successful coupling of the MEMS GC with MASPEX provides a strong foundation for a potential analytical tool in planetary science applications, where separation of complex sample matrices is required to address fundamental science questions. MEMS multidimensional gas

https://dx.doi.org/10.1021/acsearthspacechem.0c00131
ACS Earth Space Chem. 2020, 4, 1718−1729

chromatography (GC−GC) improves analytical capabilities even further, and its coupling with mass spectrometry will be the focus of future publications.

■ ASSOCIATED CONTENT

Supporting Information

The Supporting Information is available free of charge at https://pubs.acs.org/doi/10.1021/acsearthspacechem.0c00131.

Description of materials; linearity of response data in peak area (V·s) versus on-column mass (g); analytical column temperature profile for the five alkane mixture runs and the retention times (elution) of the alkanes; HETP vs column temperature discussion and data; MEMS GC-MS chromatograms from MASPEX Fast-Flight data software; mass spectra of other components of alkane mixture; mass spectral comparison of MASPEX data to NIST reference mass spectra (PDF)

■ AUTHOR INFORMATION

Corresponding Author

Ryan C. Blase − *Space Science and Engineering Division, Southwest Research Institute, San Antonio, Texas 78247, United States;* orcid.org/0000-0001-8364-620X; Email: rblase@swri.edu

Authors

Mark J. Libardoni − *Space Science and Engineering Division, Southwest Research Institute, San Antonio, Texas 78247, United States*

Gregory P. Miller − *Space Science and Engineering Division, Southwest Research Institute, San Antonio, Texas 78247, United States*

Kelly E. Miller − *Space Science and Engineering Division, Southwest Research Institute, San Antonio, Texas 78247, United States*

Charity M. Phillips-Lander − *Space Science and Engineering Division, Southwest Research Institute, San Antonio, Texas 78247, United States;* orcid.org/0000-0003-1064-8196

J. Hunter Waite − *Space Science and Engineering Division, Southwest Research Institute, San Antonio, Texas 78247, United States*

Christopher R. Glein − *Space Science and Engineering Division, Southwest Research Institute, San Antonio, Texas 78247, United States*

Hongbo Zhu − *Biomedical Engineering Department, University of Michigan, Ann Arbor, Michigan 48109, United States*

Abhishek Ghosh − *Biomedical Engineering Department, University of Michigan, Ann Arbor, Michigan 48109, United States;* orcid.org/0000-0001-8841-7078

Anandram Venkatasubramanian − *Biomedical Engineering Department, University of Michigan, Ann Arbor, Michigan 48109, United States*

Xudong Fan − *Biomedical Engineering Department, University of Michigan, Ann Arbor, Michigan 48109, United States;* orcid.org/0000-0003-0149-1326

Katsuo Kurabayashi − *Mechanical Engineering Department, University of Michigan, Ann Arbor, Michigan 48109, United States;* orcid.org/0000-0002-9613-3590

Complete contact information is available at: https://pubs.acs.org/10.1021/acsearthspacechem.0c00131

Notes

The authors declare no competing financial interest.

■ ACKNOWLEDGMENTS

This work was funded by NASA Grant number 80NSSC19K0611.

■ REFERENCES

(1) James, A. T.; Martin, A. J. P. Gas-Liquid Partition Chromatography: The Separation and Microestimation of Volatile Fatty Acids from Formic Acid to Dodecanoic Acid. *Biochem. J.* **1952**, *50*, 679−690.

(2) Holmes, J. C.; Morrell, F. A. Oscillographic Mass Spectrometric Monitoring of Gas Chromatography. *Appl. Spectrosc.* **1957**, *11*, 86−87.

(3) Gohlke, R. S. Time-of-Flight Mass Spectrometry and Gas-Liquid Partition Chromatography. *Anal. Chem.* **1959**, *31*, 535−541.

(4) Martin, A. J. P.; Synge, R. L. M. A New Form of Chromatogram Employing Two Liquid Phases. *Biochem. J.* **1941**, *35*, 1358−1368.

(5) Tal'roze, V. L.; Skurat, V. E.; Karpov, G. V. The Application of a Mass Spectrometer with a Capillary Inlet System as a Detector in a Liquid Chromatograph. *Russ. J. Phys. Chem. A* **1969**, *43*, 241−242.

(6) Tal'roze, V. L.; Skurat, V. E.; Gorodetskii, I. G.; Zolotoi, N. B. Glass and Quartz Capillary Nozzles for Mass-Spectrometer Liquid Sample Injector. *Russ. J. Phys. Chem. A* **1972**, *46*, 456−458.

(7) Baldwin, M. A.; McLafferty, F. W. Liquid Chromatography-Mass Spectrometry Interface-I: The Direct Introduction of Liquid Solutions into a Chemical Ionization Mass Spectrometer. *Org. Mass Spectrom.* **1973**, *7*, 1111−1112.

(8) Baldwin, M. A.; McLafferty, F. W. Direct Chemical Ionization of Relatively Involatile Samples. Application to Underivatized Oligopeptides. *Org. Mass Spectrom.* **1973**, *7*, 1353−1356.

(9) Tiselius, A. A New Apparatus for Electrophoretic Analysis of Colloidal Mixtures. *Trans. Faraday Soc.* **1937**, *33*, 524−531.

(10) Olivares, J. A.; Nguyen, N. T.; Yonker, C. R.; Smith, R. D. On-Line Mass Spectrometric Detection for Capillary Zone Electrophoresis. *Anal. Chem.* **1987**, *59*, 1230−1232.

(11) Thomson, J. J.; Rutherford, E. On the Passage of Electricity through Gases Exposed to Rontgen. *London, Edinburgh Dublin Philos. Mag. J. Sci.* **1896**, *42*, 392.

(12) Zeleny, J. The Velocity of the Ions Produced in Gases by Rontgen Rays. *Philos. Trans. R. Soc. A* **1900**, *195*, 193−234.

(13) McDaniel, E. W.; Martin, D. W.; Barnes, W. S. Drift Tube-Mass Spectrometer for Studies of Low-Energy Ion-Molecule Reactions. *Rev. Sci. Instrum.* **1962**, *33*, 2−7.

(14) Oyama, V. I.; Carle, G. C.; Woeller, F.; Pollack, J. B. Laboratory Corroboration of the Pioneer Venus Gas Chromatograph Analyses. *Science* **1979**, *205*, 52−54.

(15) Gel'man, B. G.; Zolotukhin, V. G.; Lamonov, N. I.; Levchuk, B. V.; Mukhin, L. M.; Nenarokov, D. F.; Okhotnikov, B. P.; Rotin, V. A.; Lipatov, A. I. Venera 12 Analysis of Venus Atmospheric Composition by Gas Chromatography. *Astron. Lett.* **1979**, *5*, 116−118.

(16) Palmer, P. T.; Limero, T. F. Mass Spectrometry in the U.S. Space Program: Past, Present, and Future. *J. Am. Soc. Mass Spectrom* **2001**, *12*, 656−675.

(17) Ren, Z.; Guo, M.; Cheng, Y.; Wang, Y.; Sun, W.; Zhang, H.; Dong, M.; Li, G. A Review of the Development and Application of Space Miniature Mass Spectrometers. *Vacuum* **2018**, *155*, 108−117.

(18) Arevalo, R., Jr.; Ni, Z.; Danell, R. M. Mass Spectrometry and Planetary Exploration: A Brief Review and Future Projection. *J. Mass Spectrom.* **2020**, *55*, No. e4454.

(19) Rushneck, D. R.; Diaz, A. V.; Howarth, D. W.; Rampacek, J.; Olson, K. W.; Dencker, W. D.; Smith, P.; McDavid, L.; Tomassian, A.; Harris, M.; Bulota, K.; Biemann, K.; LaFleur, A. L.; Biller, J. E.; Owen, T. Viking Gas Chromatograph-Mass Spectrometer. *Rev. Sci. Instrum.* **1978**, *49*, 817−834.

(20) Niemann, H. B.; Atreya, S. K.; Bauer, S. J.; Biemann, K.; Block, B.; Carignan, G. R.; Donahue, T. M.; Frost, R. L.; Gautier, D.;

Haberman, J. A.; Harpold, D.; Hunten, D. M.; Israel, G.; Lunine, J. I.; Mauersberger, K.; Owen, T. C.; Raulin, F.; Richards, J. E.; Way, S. H. The Gas Chromatograph Mass Spectrometer for the Huygens Probe. *Space Sci. Rev.* **2002**, *104*, 553−591.
(21) Wright, I. P.; Barber, S. J.; Morgan, G. H.; Morse, A. D.; Sheridan, S.; Andrews, D. J.; Maynard, J.; Yau, D.; Evans, S. T.; Leese, M. R.; Zarnecki, J. C.; Kent, B. J.; Waltham, N. R.; Whalley, M. S.; Heys, S.; Drummond, D. L.; Edeson, R. L.; Sawyer, E. C.; Turner, R. F.; Pillinger, C. T. Ptolemy−An Instrument to Measure Stable Isotopic Ratios of Key Volatiles on a Cometary Nucleus. *Space Sci. Rev.* **2007**, *128*, 363−381.
(22) Mahaffy, P. R.; Webster, C. R.; Cabane, M.; Conrad, P. G.; Coll, P.; Atreya, S. K.; Arvey, R.; Barciniak, M.; Benna, M.; Bleacher, L.; Brinckerhoff, W. B.; Eigenbrode, J. L.; Carignan, D.; Cascia, M.; Chalmers, R. A.; Dworkin, J. P.; Errigo, T.; Everson, P.; Franz, H.; Farley, R.; Feng, S.; Frazier, G.; Freissinet, C.; Glavin, D. P.; Harpold, D. N.; Hawk, D.; Holmes, V.; Johnson, C. S.; Jones, A.; Jordan, P.; Kellogg, J.; Lewis, J.; Lyness, E.; Malespin, C. A.; Martin, D. K.; Maurer, J.; McAdam, A. C.; McLennan, D.; Nolan, T. J.; Noriega, M.; Pavlov, A. A.; Prats, B.; Raaen, E.; Sheinman, O.; Sheppard, D.; Smith, J.; Stern, J. C.; Tan, F.; Trainer, M.; Ming, D. W.; Morris, R. V.; Jones, J.; Gundersen, C.; Steele, A.; Wray, J.; Botta, O.; Leshin, L. A.; Owen, T.; Battel, S.; Jakosky, B. M.; Manning, H.; Squyres, S.; Navarro-González, R.; McKay, C. P.; Raulin, F.; Sternberg, R.; Buch, A.; Sorensen, P.; Kline-Schoder, R.; Coscia, D.; Szopa, C.; Teinturier, S.; Baffes, C.; Feldman, J.; Flesch, G.; Forouhar, S.; Garcia, R.; Keymeulen, D.; Woodward, S.; Block, B. P.; Arnett, K.; Miller, R.; Edmonson, C.; Gorevan, S.; Mumm, E. The Sample Analysis at Mars Investigation and Instrument Suite. *Space Sci. Rev.* **2012**, *170*, 401−478.
(23) Hofer, L.; Wurz, P.; Buch, A.; Cabane, M.; Coll, P.; Coscia, D.; Gerasimov, M.; Lasi, D.; Sapgir, A.; Szopa, C.; Tulej, M. Prototype of the Gas Chromatograph-Mass Spectrometer to Investigate Volatile Species in the Lunar Soil for the Luna-Resurs Mission. *Planet. Space Sci.* **2015**, *111*, 126−133.
(24) Lambertus, G.; Elstro, A.; Sensenig, K.; Potkay, J.; Agah, M.; Scheuering, S.; Wise, K.; Dorman, F.; Sacks, R. Design, Fabrication, and Evaluation of Microfabricated Columns for Gas Chromatography. *Anal. Chem.* **2004**, *76*, 2629−2637.
(25) Li, M. W. H.; She, J.; Zhu, H.; Li, Z.; Fan, X. Microfabricated Porous Layer Open Tubular (PLOT) Column. *Lab Chip* **2019**, *19*, 3979−3987.
(26) Li, M. W. H.; Zhu, H.; Zhou, M.; She, J.; Li, Z.; Kurabayashi, K.; Fan, X. Peak Focusing Based on Stationary Phase Thickness Gradient. *J. Chromatogr. A* **2020**, *1614*, No. 460737.
(27) Li, M. W. H.; Huang, X.; Zhu, H.; Kurabayashi, K.; Fan, X. Microfabricated Ionic Liquid Column for Separations in Dry Air. *J. Chromatogr. A* **2020**, *1620*, No. 461002.
(28) Liu, J.; Sun, Y.; J. Howard, D.; Frye-Mason, G.; K. Thompson, A.; Ja, S.; Wang, S.-K.; Bai, M.; Taub, H.; Almasri, M.; Fan, X. Fabry−Pérot Cavity Sensors for Multipoint On-Column Micro Gas Chromatography Detection. *Anal. Chem.* **2010**, *82*, 4370−4375.
(29) Reddy, K.; Guo, Y.; Liu, J.; Lee, W.; Khaing Oo, M. K.; Fan, X. Rapid, Sensitive, and Multiplexed on-Chip Optical Sensors for Micro-Gas Chromatography. *Lab Chip* **2012**, *12*, 901−905.
(30) Zhu, H.; Nidetz, R.; Zhou, M.; Lee, J.; Buggaveeti, S.; Kurabayashi, K.; Fan, X. Flow-through Microfluidic Photoionization Detectors for Rapid and Highly Sensitive Vapor Detection. *Lab Chip* **2015**, *15*, 3021−3029.
(31) Lee, J.; Zhou, M.; Zhu, H.; Nidetz, R.; Kurabayashi, K.; Fan, X. In Situ Calibration of Micro-Photoionization Detectors in a Multi-Dimensional Micro-Gas Chromatography System. *Analyst* **2016**, *141*, 4100−4107.
(32) Lee, J.; Zhou, M.; Zhu, H.; Nidetz, R.; Kurabayashi, K.; Fan, X. Fully Automated Portable Comprehensive 2-Dimensional Gas Chromatography Device. *Anal. Chem.* **2016**, *88*, 10266−10274.
(33) Chen, D.; Hwan Seo, J.; Liu, J.; Kurabayashi, K.; Fan, X. Smart Three-Dimensional Gas Chromatography. *Anal. Chem.* **2013**, *85*, 6871−6875.
(34) Seo, J. H.; Kim, S. K.; Zellers, E. T.; Kurabayashi, K. Microfabricated Passive Vapor Preconcentrator/Injector Designed for Microscale Gas Chromatography. *Lab Chip* **2012**, *12*, 717−724.
(35) Seo, J. H.; Liu, J.; Fan, X.; Kurabayashi, K. Effect of Thermal Desorption Kinetics on Vapor Injection Peak Irregularities by a Microscale Gas Chromatography Preconcentrator. *Anal. Chem.* **2012**, *84*, 6336−6340.
(36) Kim, S.-J.; Serrano, G.; D. Wise, K.; Kurabayashi, K.; T. Zellers, E. Evaluation of a Microfabricated Thermal Modulator for Comprehensive Two-Dimensional Microscale Gas Chromatography. *Anal. Chem.* **2011**, *83*, 5556−5562.
(37) Blase, R. C.; Patrick, E. L.; Mitchell, J. N.; Libardoni, M. Analysis of Cave Atmospheres by Comprehensive Two-Dimensional Gas Chromatography (GCxGC) with Flame Ionization Detection (FID). *Anal. Chem. Res.* **2015**, *3*, 54−62.
(38) Libardoni, M.; Blase, R. C. Laser Thermal Desorption and GC x GC for Harsh Environment and Planetary Mass Spectrometry. *Curr. Trends Mass Spectrom* **2019**, *17*, 16−22.
(39) Brockwell, T. G.; Meech, K. J.; Pickens, K.; Waite, J. H.; Miller, G.; Roberts, J.; Lunine, J. I.; Wilson, P. In *The Mass Spectrometer for Planetary Exploration (MASPEX)*, IEEE Aerospace Conference Proceedings; IEEE Computer Society, 2016.
(40) Glein, C. R.; Waite, J. H.; Miller, K. E. In *MAss Spectrometer for Planetary EXploration-ORganic Composition Analyzer (MASPEX-ORCA) for Europa Lander and Other Missions to Icy Ocean Worlds*, 2019 Astrobiology Science Conference; Seattle, Washington, 2019.
(41) Glein, C. R.; Zolotov, M. Y. Hydrogen, Hydrocarbons, and Habitability Across the Solar System. *Elements* **2020**, *16*, 47−52.
(42) Waite, J. H.; Glein, C. R.; Perryman, R. S.; Teolis, B. D.; Magee, B. A.; Miller, G.; Grimes, J.; Perry, M. E.; Miller, K. E.; Bouquet, A.; Lunine, J. I.; Brockwell, T.; Bolton, S. J. Cassini Finds Molecular Hydrogen in the Enceladus Plume: Evidence for Hydrothermal Processes. *Science* **2017**, *356*, 155−159.
(43) Postberg, F.; Khawaja, N.; Abel, B.; Choblet, G.; Glein, C. R.; Gudipati, M. S.; Henderson, B. L.; Hsu, H. W.; Kempf, S.; Klenner, F.; Moragas-Klostermeyer, G.; Magee, B.; Nölle, L.; Perry, M.; Reviol, R.; Schmidt, J.; Srama, R.; Stolz, F.; Tobie, G.; Trieloff, M.; Waite, J. H. Macromolecular Organic Compounds from the Depths of Enceladus. *Nature* **2018**, *558*, 564−568.
(44) Eigenbrode, J. L.; Summons, R. E.; Steele, A.; Freissinet, C.; Millan, M.; Navarro-González, R.; Sutter, B.; McAdam, A. C.; Franz, H. B.; Glavin, D. P.; Archer, P. D.; Mahaffy, P. R.; Conrad, P. G.; Hurowitz, J. A.; Grotzinger, J. P.; Gupta, S.; Ming, D. W.; Sumner, D. Y.; Szopa, C.; Malespin, C.; Buch, A.; Coll, P. Organic Matter Preserved in 3-Billion-Year-Old Mudstones at Gale Crater, Mars. *Science* **2018**, *360*, 1096−1101.
(45) Mastrogiuseppe, M.; Poggiali, V.; Hayes, A. G.; Lunine, J. I.; Seu, R.; Mitri, G.; Lorenz, R. D. Deep and Methane-Rich Lakes on Titan. *Nat. Astron.* **2019**, *3*, 535−542.
(46) Grady, M. M.; Wright, I. P.; Engrand, C.; Siljestrom, S. The Rosetta Mission and the Chemistry of Organic Species in Comet 67P/Churyumov-Gerasimenko. *Elements* **2018**, *14*, 95−100.
(47) Rubin, M.; Altwegg, K.; Balsiger, H.; Bertherlier, J.-J.; Combi, M. R.; De Keyser, J.; Drozdovskaya, M.; Fiethe, B.; Fuselier, S. A.; Gasc, S.; Gombosi, T. I.; Hanni, N.; Hansen, K. C.; Mall, U.; Reme, H.; Schroeder, I. R. H. G.; Schuhmann, M.; Semon, T.; Waite, J. H.; Wampfler, S. F.; Wurz, P. Elemental and Molecular Abundances in Comet 67P/Churyumov-Gerasimenko. *Mon. Not. R. Astron. Soc.* **2019**, *489*, 594−607.
(48) Stern, S. A.; Grundy, W. M.; McKinnon, W. B.; Weaver, H. A.; Young, L. A. The Pluto System After New Horizons. *Annu. Rev. Astron. Astrophys.* **2018**, *56*, 357−392.
(49) Gladstone, G. R.; Stern, S. A.; Ennico, K.; Olkin, C. B.; Weaver, H. A.; Young, L. A.; Summers, M. E.; Strobel, D. F.; Hinson, D. P.; Kammer, J. A.; Parker, A. H.; Steffl, A. J.; Linscott, I. R.; Parker, J. W.; Cheng, A. F.; Slater, D. C.; Versteeg, M. H.; Greathouse, T. K.; Retherford, K. D.; Throop, H.; Cunningham, N. J.; Woods, W. W.; Singer, K. N.; Tsang, C. C. C.; Schindhelm, E.; Lisse, C. M.; Wong, M. L.; Yung, Y. L.; Zhu, X.; Curdt, W.; Lavvas, P.; Young, E. F.; Tyler,

https://dx.doi.org/10.1021/acsearthspacechem.0c00131
ACS Earth Space Chem. 2020, 4, 1718−1729

G. L.; et al. The Atmosphere of Pluto as Observed by New Horizons. *Science* **2016**, *351*, No. aad8866.
(50) Abplanalp, D.; Wurz, P.; Huber, L.; Leya, I. An Optimised Compact Electron Impact Ion Storage Source for a Time-of-Flight Mass Spectrometer. *Int. J. Mass Spectrom.* **2010**, *294*, 33−39.
(51) Blase, R. C.; Llera, K.; Luspay-Kuti, A.; Libardoni, M. The Importance of Detector Acquisition Rate in Comprehensive Two-Dimensional Gas Chromatography (GC×GC). *Sep. Sci. Technol.* **2014**, *49*, 847−853.
(52) Restek. *Guide to GC Column Selection and Optimizing Separations*; Bellefonte, PA, 2013.
(53) Agilent Technologies. *GC and GC/MS Your Essential Resource for Columns & Supplies*; Santa Clara, CA, 2014.
(54) Supelco Sigma Alrdrich. *GC Column Selection Guide, Achieve Optimal Method Performance*; St. Louis, MO, 2013.
(55) Spangler, G. E. Height Equivalent to a Theoretical Plate Theory for Rectangular GC Columns. *Anal. Chem.* **1998**, *70*, 4805−4816.
(56) Lemmon, E. W.; McLinden, M. O.; Friend, and D. G. *NIST Chemistry WebBook, NIST Standard Reference Database*; NIST, 2017.
(57) NIST Chemistry WebBook. (accessed May 15, 2020), https://webbook.nist.gov/chemistry/.
(58) Eichelberger, J. W.; Harris, L. E.; Budde, W. L. Reference Compound to Calibrate Ion Abundance Measurements in Gas Chromatography-Mass Spectrometry Systems. *Anal. Chem.* **1975**, *47*, 995−1000.

https://dx.doi.org/10.1021/acsearthspacechem.0c00131
ACS Earth Space Chem. 2020, 4, 1718−1729